On the structure and chemistry of fossils of the earliest woody plant

Christine Strullu-Derrien, Sylvain Bernard, Alan R T Spencer, Laurent Remusat, Paul Kenrick, Delphine Derrien

On the structure and chemistry of fossils of the earliest woody plant

Christine Strullu-Derrien[1,2,3], Sylvain Bernard[4], Alan R.T. Spencer[1,5], Laurent Remusat[4], Paul Kenrick[1] and Delphine Derrien[6]

[1]*The Natural History Museum, Department of Earth Sciences, London, UK.*

[2]*Laboratoire of Excellence ARBRE, UMR « Tree-Microbes Interactions », INRA Nancy, France*

[3]*Institut de Systématique, Evolution, Biodiversité (ISYEB), UMR7205, Muséum National d'Histoire naturelle, Sorbonne Université, CNRS, Paris, France*

[4]*Muséum National d'Histoire Naturelle, Sorbonne Université, CNRS UMR 7590, IRD, IMPMC, Paris, France*

[5]*Department of Earth Science and Engineering, Imperial College London, UK*

[6]*Biogeochemistry of Forest Ecosystems, INRA Nancy, France*

Corresponding author: Christine Strullu-Derrien, c.strullu-derrien@nhm.ac.uk

ABSTRACT

Palaeontology relies on the description of fossil morphologies to understand the evolutionary history of life on Earth. Yet, much remains unknown about the impact of fossilization processes, even though these may introduce biases in paleobiological interpretations. Here, we report the characterization of fossilised remains of the earliest woody plant *Armoricaphyton chateaupannense* preserved either in 2D (as flat carbonaceous films) or in 3D (as organo-mineral structures) in early Devonian shales (ca 407 Ma) of the Armorican Massif on the northern margin of Gondwana. To document the fine-scale structure and the chemistry of the tracheids of this ancient plant, we used propagation phase contrast synchrotron radiation X-ray microcomputed tomography (PPC-SRµCT), transmission electron microscopy (TEM) and synchrotron-based scanning transmission X-ray microscopy (STXM) coupled with X-ray absorption near edge structure (XANES) spectroscopy. PPC-SRµCT enables digital visualization of cell walls in unprecedented detail for the specimens preserved in 3D revealing structures similar to those observed in extant lignified cells, thereby strongly suggesting that the earliest woody plant *A. chateaupannense* originally contained lignin-like compounds. STXM-based XANES and TEM data show that, whatever the preservation modes (3D vs 2D), the original lignin or lignin-like compounds, if present, did not withstand fossilization processes and were replaced by

pyrobitumen compounds containing automorphic Ti-nanominerals. Altogether, the present study illustrates that anatomical and chemical preservations may not always be correlated.

Keywords: Earliest Woody Plant, Lignin, Fossilization, Pyrobitumen, Microtomography, XANES spectroscopy .

INTRODUCTION

The fossil record provides information fundamental to understanding the evolution and diversification of plants on land. One key source of data comes from tissue systems and their preserved cellular constituents. By drawing comparison to modern species, one can infer aspects of function, physiology and chemical composition. In addition, direct chemical analyses of fossil residues could help interpreting the nature of fossilized tissues. However, assessments of chemical signals remain difficult, notably because fossilization processes inevitably modify soft tissues, altering or obscuring their original biochemical structure (Bernard and Papineau 2014; Briggs and Summons 2014), thereby hindering the precise reconstruction of their original chemistry.

Here we investigate cell structure and residual chemistry of the most ancient woody plant *Armoricaphyton chateaupannense* (ca 407Ma) from the Armorican Massif, Western France (Strullu-Derrien 2010; Gerrienne *et al.* 2011; Strullu-Derrien *et al.* 2014) Phylogenetically, this plant is closely related to *Tetraxylopteris*, a genus of extinct vascular plants that belonged to Lignophytes, i.e. plants producing wood through a cambium (Strullu-Derrien 2010). In modern woody plants, tracheid cell walls are composed primarily of cellulose, hemicelluloses and lignin. Lignin is a class of complex organic macromolecules that lend rigidity to cell walls making them less permeable to water, thereby improving conductivity within the vascular system. The composition of lignin varies from species to species. What kind of lignin was synthetized by *A. chateaupannense* (e.g. the most ancient woody plant) remains an open question.

Over the past ten years, the use of advanced techniques has shown that diagenesis does not systematically obliterate all the biochemical information carried by fossils (Bernard *et al.* 2007; Lepot *et al.* 2008; Steemans *et al.* 2010; Cosmidis *et al.* 2013*b*, *a*; Alleon *et al.* 2016*a*, 2018; Delarue *et al.* 2017, 2018; Abbott *et al.* 2017). In parallel, laboratory experiments have highlighted that burial-induced thermal degradation of organic molecules can be more abstruse than generally believed (Schiffbauer *et al.* 2012; Li *et al.* 2013, 2014; McNamara *et al.* 2013*a*,

b; Bernard *et al.* 2015; Alleon *et al.* 2016*b*, 2017; Miot *et al.* 2017; Vinogradoff *et al.* 2018). Yet the impact of advanced fossilization processes remains poorly constrained, limiting the significance of chemical studies.

Here, to go further than previous studies conducted on fossil tracheids of different species (Edwards et al., 1997; Boyce et al., 2001, 2002, 2003, 2010; Bernard et al., 2009, 2010 Galvez et al., 2012a; Abbott et al., 2017) we combined non-invasive synchrotron-based microtomography and spectromicroscopy tools to document, at the submicrometer scale, both the cell wall structure and the chemical nature of the organic components of specimens of *A. chateaupannense* preserved either in 2D (i.e. as flat carbonaceous films) or in 3D (i.e. as organo-mineral structures). Based on these observations, we reconstruct the fine anatomy of the plant tracheids and constrain the diagenetic history of the fossils and we discuss the significance of the biogeochemical signals retrieved.

GEOLOGICAL SETTING

Specimens of the early Devonian plant *A. chateaupannense* (407 Ma) preserved in 2D (i.e. as flat carbonaceous films; Fig. 1a) or 3D (i.e. as organo-mineral structures; Fig. 1b) were recovered from the Châteaupanne quarry (47°22’11.73’’N/0°49’31.97’’W) located in the Armorican Massif (France). The Armorican Massif is the western part of the Variscan Belt that extended throughout central Europe during the Late Paleozoic (Ballèvre *et al.* 2009).

The Châteaupanne unit belongs to the South Armorican domain and consists of Ordovician marine sediments unconformably overlain by the Devonian (Emsian Stage) Chalonnes Formation (Fig. 1d). This formation, located on the northern margin of Gondwana during the Devonian, is predominantly composed of massive limestone overlying terrigeneous layers (Fig. 1d), suggesting deposition in a nearshore environment (Strullu-Derrien *et al.* 2010). Both types of specimens of *A. chateaupannense* were collected from these terrigeneous layers.

Mineralogical Context

The mineral matrix surrounding the fossil specimens mainly comprises submicrometric K-aluminosilicates, with Fe-aluminosilicates locally concentrated in thin veins (Figs 2a,b). Quartz (SiO2), rutile/anatase (TiO2) and Al-phosphates containing traces of Cerium are also observed (Figs 2b,c). Both specimens of fossil plant possess an organic component, the specimens preserved in 3D are also heavily pyritized.

MATERIAL AND METHODS

Propagation Phase Contrast X-Ray Synchrotron Microtomography

Propagation phase contrast X-ray synchrotron microtomography (PPC-SRμCT) was employed to study the three-dimensional structure of the permineralized wood, using the ID19 beamline of the European Synchrotron Radiation Facility (ESRF), Grenoble, France (Feist *et al.* 2005). The acquired tomographic dataset (0.551 μm per voxel) was converted to 8-bit grayscale bitmapped images using ImageJ (Abramoff *et al.* 2004). It was then imported using DrishtiImport v2.5 (Limaye 2012) and converted into the proprietary (.pvl.nc) volume format used by the volume exploration and presentation tool Drishti v2.5. Drishti volume renders the dataset voxels into a manipulable 3D model. The volume was false coloured by mapping voxel x-ray attenuation values to colour ranges, each targeting a different mineralogical x-ray attenuation range; this enables the extraction of pyrite from the surrounding matrix through digital thresholding (Spencer et al, 2017). Clipping planes were used to crop the volume to smaller areas of interest. Drishti has built-in scalebars and bounding boxes that were used to measure the real-word size of features within the 3D model space. The Keyframe Editor was used to produce animated image sequences showing the rendered 3D model. The individual animation was produced into a video using the open-source animation package Blender™ (Garwood and Dunlop 2014).

Preparation of Ultrathin Foils of Samples

Focused Ion Beam (FIB) milling is commonly used for preparing ultrathin samples for STXM and TEM investigations since it allows extracting, *in situ*, ultrathin foils of sample with a very high spatial precision (Schiffbauer and Xiao 2009; Wirth 2009). Here, FIB foils (~20μm x 5μm x 80 nm) were extracted from the organic parts of the specimens investigated using a Zeiss Auriga FIB system (IPGP, Paris, France). The FIB lift-out extraction procedure maintains textural integrity, even in the case of loosely consolidated materials, and prevents shrinkage and deformation of microscale to nanoscale pores, even in the case of highly sensitive materials (Schiffbauer and Xiao 2009; Wirth 2009). Milling at low Ga-ion currents prevents common artefacts like creation of cracks or amorphous layers, redeposition of the sputtered material and significant changes in the speciation of complex carbon-based polymers (Bernard *et al.* 2009; Bassim *et al.* 2012).

Scanning Transmission Electron Microscopy (STEM)

STEM observations were performed with a JEOL 2100 Field Emission Gun (FEG) microscope (IMPMC - Paris, France) operating at 200 kV. Scanning Transmission Electron Microscopy (STEM) Z-contrast imaging was performed using the high-angle annular dark field (HAADF) mode. High-resolution TEM (HRTEM) images were collected using the bright field mode allowing us to resolve the crystalline planes (of the order of 0.1 nm) of the different phases. Elemental compositions of different phases were determined by energy dispersive X-ray spectrometry (EDXS) performed using the JEOL detector with an ultrathin window allowing detection of light elements.

X-Ray Absorption Near Edge Structure Spectroscopy (XANES)

XANES data were collected using a scanning transmission X-ray microscope (Cosmidis and Benzerara 2014; Karunakaran *et al.* 2015), on both the 10ID-1 STXM beamline (Kaznatcheev *et al.* 2007) at the Canadian Light Source (CLS) and on the HERMES STXM beamline (Belkhou *et al.* 2015; Swaraj *et al.* 2017) at the synchrotron SOLEIL for all the specimens investigated. At CLS, a 100 nm thick titanium filter was used to remove the contribution of second order light while at SOLEIL, beamline optical elements were exposed to a continuous flow of pure O_2 to remove carbon contamination. Energy calibration was done before measurements using the well-resolved 3p Rydberg peak of gaseous CO_2 at 294.96 eV. XANES data were extracted from image stacks collected at energy increments of 0.1 eV over the carbon (270–350 eV) absorption range with a dwell time of ≤ 1 ms per pixel to prevent irradiation damage (Wang *et al.* 2009). Alignment of images of stacks and extraction of XANES spectra were done using the latest version aXis2000 software. The C-XANES spectra shown in the present contribution correspond to homogeneous carbon-rich areas of several hundreds of square nanometres and were normalized to the carbon quantity by integrating the spectra (after subtraction of a power law background) from the pre-edge region up to the mean ionization energy (e.g. 282-291.5 eV at the C K edge) following the method proposed and validated by Le Guillou et al. (2018).

RESULTS

Anatomical Details

Although fine-scale anatomical details of specimens preserved in 2D cannot be observed, specimens preserved in 3D reveal cellular details of the vascular system (Fig. 3). The tracheids have a radial diameter of ca 30–69 µm ($\bar{x}$ 46 µm), a tangential diameter of ca 20–50 µm ($\bar{x}$ 32 µm) and a length exceeding 1.2 mm (Figs 3a,b). Virtually removing the pyrite reveals that the tracheids possess scalariform bordered pits (Figs 3b-i), typical of P-type tracheids (Kenrick and Crane 1997; Strullu-Derrien *et al.* 2013). Similarly to modern lignified tissues, the cell walls comprise secondary wall thickenings (ca 5 µm) between the pits, consisting of an external layer (0.4–1.0 µm thick; $\bar{x}$ 0.6 µm) interpreted as decay resistant and an internal hollow (1.7–5.0 µm diameter; $\bar{x}$ 3.1 µm) presumably corresponding to a less resistant layer (Figs 3d,e) (Kenrick and Edwards 1988). In contrast to modern groups, an additional perforate sheet of secondary wall material overlies the pit apertures (Figs 3f,g), as observed in P-type tracheids (Kenrick and Crane 1997; Strullu-Derrien *et al.* 2013). The perforations are distributed in a reticulum (Fig. 3g) and have a highly variable shape ranging from 0.9–3.6 µm ($\bar{x}$ 2.3 µm) in diameter. A similar pattern of pitting was observed on the four facets of the tracheid cell walls (Figs 3h,i; movie S1).

Organic Carbon Speciation

The specimens investigated, either preserved in 3D or in 2D, are very homogeneous and similar in terms of carbon speciation (Fig. 4a). Their C-XANES spectra show a broad absorption feature at ~ 284.8 eV indicating the presence of aromatic or olefinic carbons, a peak at 286.3 eV that can be attributed to carbons bonded to oxygen or sulfur, and a peak at ~ 288.4 eV, likely corresponding to the presence of ester or carboxylic groups (Bernard *et al.* 2015; Karunakaran *et al.* 2015; Le Guillou *et al.* 2018). An additional gentle absorption feature at 287.3 eV that can be attributed to the presence of phenols or ketones was observed for specimens preserved in 3D.

Mineral Inclusions

The specimens investigated, either preserved in 3D or in 2D, exhibit needle-shape, automorphic nanocrystals (~ 50 nm) of titanium oxides (likely rutile or anatase) homogeneously and ubiquitously distributed within the organic carbon (Figs 4b,c,e). Of note, all the observed organic material contains these Ti-nanominerals; they are ubiquitous in these fossils. Specimens preserved in 2D also contain submicrometric Ca-nanominerals (likely calcite) and Fe-nanominerals (likely pyrite and iron oxides/hydroxides) (Figs 4d,f).

DISCUSSION

The anatomical details of the specimens preserved in 3D likely results from the early pyritization of the tissues, which was very much less prevalent in the specimens preserved in 2D. Pyritization of plant tissues may remain incomplete, the distribution of pyrite in fossil plants being generally interpreted in terms of differential biodegradability of the original organic constituents of the plant (Kenrick and Edwards 1988; Edwards *et al.* 1997; Grimes *et al.* 2001; Bernard *et al.* 2010; Cai *et al.* 2012; Schiffbauer *et al.* 2014). The pattern of secondary cell wall thickenings interspersed by very regular perforations revealed by tomography (Fig. 3) strongly suggests that *A. chateaupannense* was originally constituted of two different organic phases, one being more easily biodegradable than the other. It may therefore be assumed that, in addition to biodegradable cellulose, the tracheid cell walls of *A. chateaupannense* originally contained decay-resistant lignin-like compounds.

Historically, cell-wall biopolymers such as lignin have been seen as intrinsically more resistant to biodegradation and thermal maturation than polysaccharides and proteins for instance (Tegelaar *et al.* 1989; Eglinton and Logan 1991; van Bergen *et al.* 1995; Briggs 1999; Derenne and Largeau 2001). This view has since been challenged by studies that demonstrated that the persistence of organic compounds is not only controlled by their molecular structure, but rather mainly by biological and environmental factors (Schmidt *et al.* 2011; Lehmann and Kleber 2015; Keiluweit *et al.* 2016). Rot fungi in the Agaricomycetes have the ability to decompose lignin (Floudas *et al.* 2012; Krah *et al.* 2018), so do some modern bacteria (Ma *et al.* 2016; Wilhelm *et al.* 2018). Although thermodynamic constraints prevent the biodegradation of lignin under anaerobic conditions (Keiluweit *et al.* 2016), fungal or bacterial lineages capable of lignin degradation likely already existed during the early Devonian (Nelsen et al., 2016). It has also been recognized that the primary structure of the lignin molecule may thermally degrade even at relatively low temperature (Cody and Sághi-Szabó 1999), making lignin residues difficult to identify in the fossil record.

All the specimens investigated are homogeneous in terms of carbon speciation and exhibit a similar molecular structure (Fig. 4a). These compounds are quite different from modern lignin (Fig. 4a) or thermally degraded lignin (Edwards *et al.* 1997; Boyce *et al.* 2002, 2003, 2010; Bernard *et al.* 2010; Galvez *et al.* 2012*b*; Karunakaran *et al.* 2015), and rather typical of macromolecular aromatic compounds such as pyrobitumen (Bernard *et al.* 2012*b*, *a*; Bernard and Horsfield 2014) (Fig. 4a). In other words, whatever the preservation mode (3D vs 2D), the original lignin or lignin-like compounds, if present, did not withstand fossilization processes and were replaced by pyrobitumen.

The presence of Ti-nanominerals within the organic compounds of all the specimens investigated (Figs. 4b,c,e) may help to constrain the geological processes that affected the original organic molecules of the fossils. There is no doubt that these Ti-nanominerals were not originally present within the *A. chateaupannense* vascular tissues. In fact, besides Ti accumulation in plants that grow on Ti-rich soils (Ramakrishna *et al.* 1989), no Ti-rich phytolith has ever been reported. Relatively common in hydrothermal veins (Rumble *et al.* 1986; Craw 2002), association of Ti with organic compounds has previously been reported for plant fossils (Pe-Piper *et al.* 2011; Galvez *et al.* 2012*a*) and other ancient organic fossils (Lekele Baghekema *et al.* 2017; Wacey *et al.* 2018), and interpreted as diagenetic features. Here, the euhedral needle shape, narrow size distribution, and lack of alteration features of the Ti-nanominerals observed within the organic compounds of all the specimens support their authigenic growth rather than a detrital origin.

Titanium may be mobile in relatively shallow diagenetic settings in the presence of complexing organic acids (Hausrath *et al.* 2009; Galvez *et al.* 2012*a*). Here, the biodegradation of organic tissues trapped in the sediment likely produced organic acids that promoted Ti solubility and transport in the form of organic complexes (Huggins and Huffman 2004). These complexes have eventually been trapped into the tracheid scaffolding of the specimens investigated and, during subsequent burial, experienced pyrolitic dissociation into pyrobitumen-like compounds and Ti-nanominerals.

The homogeneous chemical composition of the organic component of the specimens investigated, whatever their preservation mode, together with the homogeneous and ubiquitous distribution of the Ti-nanominerals down to the submicrometric scale attest that the original biopolymers of *A. chateaupannense* did not withstand the fossilization processes. In fact, if a significant proportion of the original biopolymers had been preserved in the fossils, some variability might have been expected (Boyce et al. 2002, 2010), both in terms of organic speciation and distribution of Ti-nanominerals, which is not the case.

Our findings illustrate the difficulty of retrieving information on the primary chemistry of organisms preserved as fossils. Biopolymers inevitably experience degradation depending on the physical and chemical conditions that prevail during fossilization and burial. Here, despite the loss of the original biopolymers and their replacement by pyrobitumen compounds containing Ti-nanominerals, the fine scale cellular structure of the vascular tissues of *A. chateaupannense* is exceptionally preserved. This study shows that pyrite formed during early diagenesis preserved the 3D anatomical framework of the plant tracheids. It also demonstrates that the replacement of biopolymers by pyrobitumen constitutes a diagenetic pathway relevant for the morphological

preservation of fossil plant tissues with varied structural outcomes, encompassing fossils in which cellular level details are preserved and those in which they are not.

ACKNOWLEDGEMENTS

We gratefully acknowledge financial support from the ERC project PaleoNanoLife (Grant 161764), the LabEx ARBRE Nancy (ANR-11-LABX-0002-01), the Palaeontological Association, UK (Grant PA - RG201602), the LabEx BCDiv Paris (ANR-10-LABX-0003) and the Fondation Mécènes et Loire, Angers (France). We thank Stephan Borensztajn (IPGP) for the preparation of FIB sections, Jean-Michel Guigner (IMPMC) for his expert support with the TEM and Matthieu Harlaux for helpful discussion. Special thanks go to Paul Tafforeau (ESRF), Jian Wang (CLS), Yingshen Lu (CLS), Stefan Stanescu (SOLEIL) and Sufal Swaraj (SOLEIL) for their expert support with the microtomography and the STXM beamlines. The TEM facility at IMPMC is supported by Région Ile de France grant SESAME 2000 E 1435. The ID19 beamline (ESRF) is supported by the EPN science campus and 22 countries. The 10ID-1 beamline (CLS) is supported by the NSERC, the CIHR, the NRC and the University of Saskatchewan. The HERMES beamline (SOLEIL) is supported by the CNRS, the CEA, the Region Ile de France, the Departmental Council of Essonne and the Region Centre (France).

AUTHOR CONTRIBUTIONS

C.S-D, **S.B.** and **L.R.** designed and funded the present research. **C.S-D.** collected the specimens investigated. **A.R.T.S.** performed the PPC-SRµCT reconstructions and interpret them with **C.S-D**. **S.B.** performed the STXM and TEM experiments. **C.S-D., S.B., L.R., P.K.** and **D.D.** interpreted the data and discussed their implications. **C.S-D., S.B and D.D.** wrote the present article with critical inputs from the other co-authors.

The specimens belong to CS-D's collection and are provisionally housed at the Museum Angers. The numbers are: CSD-07M-01 (Fig. 1a), CSD-06C-02 (Fig. 1b), CSD-07F-01 (Fig. 2), CSD-017-01 (FIB lamella, Fig. 1e-g), CSD-017-02 (FIB lamella, Fig. 3).

REFERENCES

ABBOTT, G. D., FLETCHER, I. W., TARDIO, S. and HACK, E. 2017. Exploring the geochemical distribution of organic carbon in early land plants: a novel approach. *Philosophical Transactions of the Royal Society B: Biological Sciences*, **373**, 20160499.

ABRAMOFF, M. D., MAGALHAES, P. J. and RAM, S. J. 2004. Image Processing with ImageJ. *Biophotonics International*, **11**, 36–42.

ALLEON, J., BERNARD, S., LE GUILLOU, C., BEYSSAC, O., SUGITANI, K. and ROBERT, F. 2018. Chemical nature of the 3.4 Ga Strelley Pool microfossils. *Geochemical Perspectives Letters*, 37–42.

ALLEON, J., BERNARD, S., LE GUILLOU, C., DAVAL, D., SKOURI-PANET, F., KUGA, M. and ROBERT, F. 2017. Organic molecular heterogeneities can withstand diagenesis. *Scientific Reports*, **7**.

ALLEON, J., BERNARD, S., LE GUILLOU, C., MARIN-CARBONNE, J., PONT, S., BEYSSAC, O., MCKEEGAN, K. D. and ROBERT, F. 2016*a*. Molecular preservation of 1.88 Ga Gunflint organic microfossils as a function of temperature and mineralogy. *Nature Communications*, **7**, 11977.

ALLEON, J., BERNARD, S., LE GUILLOU, C., DAVAL, D., SKOURI-PANET, F., PONT, S., DELBES, L. and ROBERT, F. 2016*b*. Early entombment within silica minimizes the molecular degradation of microorganisms during advanced diagenesis. *Chemical Geology*, **437**, 98–108.

BALLÈVRE, M., BOSSE, V., DUCASSOU, C. and PITRA, P. 2009. Palaeozoic history of the Armorican Massif: Models for the tectonic evolution of the suture zones. *Comptes Rendus Geoscience*, **341**, 174–201.

BASSIM, N. D., DE GREGORIO, B. T., KILCOYNE, A. L. D., SCOTT, K., CHOU, T., WIRICK, S., CODY, G. and STROUD, R. M. 2012. Minimizing damage during FIB sample preparation of soft materials: FIB SAMPLE PREPARATION OF SOFT MATERIALS. *Journal of Microscopy*, **245**, 288–301.

BELKHOU, R., STANESCU, S., SWARAJ, S., BESSON, A., LEDOUX, M., HAJLAOUI, M. and DALLE, D. 2015. HERMES: a soft X-ray beamline dedicated to X-ray microscopy. *Journal of Synchrotron Radiation*, **22**, 968–979.

BERNARD, S. and PAPINEAU, D. 2014. Graphitic Carbons and Biosignatures. *Elements*, **10**, 435–440.

337 BERNARD, S. and HORSFIELD, B. 2014. Thermal Maturation of Gas Shale Systems. *Annual*
338 *Review of Earth and Planetary Sciences*, **42**, 635–651.
339 BERNARD, S. BENZERARA, K., BEYSSAC, O. and BROWN, G. E. 2010. Multiscale
340 characterization of pyritized plant tissues in blueschist facies metamorphic rocks.
341 *Geochimica et Cosmochimica Acta*, **74**, 5054–5068.
342 BERNARD, S., WIRTH, R., SCHREIBER, A., SCHULZ, H.-M. and HORSFIELD, B. 2012*a*.
343 Formation of nanoporous pyrobitumen residues during maturation of the Barnett Shale
344 (Fort Worth Basin). *International Journal of Coal Geology*, **103**, 3–11.
345 BERNARD, S., BENZERARA, K., BEYSSAC, O., BALAN, E. and BROWN JR., G. E. 2015.
346 Evolution of the macromolecular structure of sporopollenin during thermal degradation.
347 *Heliyon*, **1**, e00034.
348 BERNARD, S., BENZERARA, K., BEYSSAC, O., BROWN, G. E., STAMM, L. G. and
349 DURINGER, P. 2009. Ultrastructural and chemical study of modern and fossil sporoderms
350 by Scanning Transmission X-ray Microscopy (STXM). *Review of Palaeobotany and*
351 *Palynology*, **156**, 248–261.
352 BERNARD, S., HORSFIELD, B., SCHULZ, H.-M., WIRTH, R., SCHREIBER, A. and
353 SHERWOOD, N. 2012*b*. Geochemical evolution of organic-rich shales with increasing
354 maturity: A STXM and TEM study of the Posidonia Shale (Lower Toarcian, northern
355 Germany). *Marine and Petroleum Geology*, **31**, 70–89.
356 BERNARD, S., BENZERARA, K., BEYSSAC, O., MENGUY, N., GUYOT, F., BROWNJR, G.
357 and GOFFE, B. 2007. Exceptional preservation of fossil plant spores in high-pressure
358 metamorphic rocks. *Earth and Planetary Science Letters*, **262**, 257–272.
359 BOYCE, C. K., HAZEN, R. M. and KNOLL, A. H. 2001. Nondestructive, in situ, cellular-scale
360 mapping of elemental abundances including organic carbon in permineralized fossils.
361 *Proceedings of the National Academy of Sciences*, **98**, 5970–5974.
362 BOYCE, C. K., ABRECHT, M., ZHOU, D. and GILBERT, P. U. P. A. 2010. X-ray photoelectron
363 emission spectromicroscopic analysis of arborescent lycopsid cell wall composition and
364 Carboniferous coal ball preservation. *International Journal of Coal Geology*, **83**, 146–153.
365 BOYCE, C. K., CODY, G. D., FESER, M., JACOBSEN, C., KNOLL, A. H. and WIRICK, S.
366 2002. Organic chemical differentiation within fossil plant cell walls detected with X-ray
367 spectromicroscopy. *Geology*, **30**, 1039.
368 BOYCE, C. K., CODY, G. D., FOGEL, M. L., HAZEN, R. M., ALEXANDER, C. M. O. and
369 KNOLL, A. H. 2003. Chemical Evidence for Cell Wall Lignification and the Evolution of

Tracheids in Early Devonian Plants. *International Journal of Plant Sciences*, **164**, 691–702.

BRIGGS, D. E. G. 1999. Molecular taphonomy of animal and plant cuticles: selective preservation and diagenesis. *Philosophical Transactions of the Royal Society B: Biological Sciences*, **354**, 7–17.

BRIGGS, D. E. G. and SUMMONS, R. E. 2014. Ancient biomolecules: Their origins, fossilization, and role in revealing the history of life: Prospects & Overviews. *BioEssays*, **36**, 482–490.

CAI, Y., SCHIFFBAUER, J. D., HUA, H. and XIAO, S. 2012. Preservational modes in the Ediacaran Gaojiashan Lagerstätte: Pyritization, aluminosilicification, and carbonaceous compression. *Palaeogeography, Palaeoclimatology, Palaeoecology*, **326**–**328**, 109–117.

CODY, G. D. and SÁGHI-SZABÓ, G. 1999. Calculation of the 13C NMR chemical shift of ether linkages in lignin derived geopolymers: *Geochimica et Cosmochimica Acta*, **63**, 193–205.

COSMIDIS, J. and BENZERARA, K. 2014. Soft x-ray scanning transmission spectromicroscopy. *In* GOWER, L. (ed.) *Biomineralization Sourcebook*, CRC Press, 115–133 pp.

COSMIDIS, J., BENZERARA, K., MENGUY, N. and ARNING, E. 2013*a*. Microscopy evidence of bacterial microfossils in phosphorite crusts of the Peruvian shelf: Implications for phosphogenesis mechanisms. *Chemical Geology*, **359**, 10–22.

COSMIDIS, J., BENZERARA, K., GHEERBRANT, E., ESTÈVE, I., BOUYA, B. and AMAGHZAZ, M. 2013*b*. Nanometer-scale characterization of exceptionally preserved bacterial fossils in Paleocene phosphorites from Ouled Abdoun (Morocco). *Geobiology*, **11**, 139–153.

CRAW, D. 2002. Geochemistry of late metamorphic hydrothermal alteration and graphitisation of host rock, Macraes gold mine, Otago Schist, New Zealand. *Chemical Geology*, **191**, 257–275.

DELARUE, F., ROBERT, F., SUGITANI, K., TARTÈSE, R., DUHAMEL, R. and DERENNE, S. 2017. Investigation of the Geochemical Preservation of *ca.* 3.0 Ga Permineralized and Encapsulated Microfossils by Nanoscale Secondary Ion Mass Spectrometry. *Astrobiology*, **17**, 1192–1202.

DELARUE, F., ROBERT, F., SUGITANI, K., TARTÈSE, R., DUHAMEL, R. and DERENNE, S. 2018. Nitrogen isotope signatures of microfossils suggest aerobic metabolism 3.0 Gyr ago. *Geochemical Perspectives Letters*, 32–36.

DERENNE, S. and LARGEAU, C. 2001. A review of some important families of refractory macromolecules: composition, origin, and fate in soils and sediments. *Soil Science*, **166**, 833–847.

DISNAR, J. R. and SUREAU, J. F. 1990. Organic matter in ore genesis: Progress and perspectives. *Organic Geochemistry*, **16**, 577–599.

EDWARDS, D., EWBANK, G. and ABBOTT, G. D. 1997. Flash pyrolysis of the outer cortical tissues in Lower Devonian Psilophyton dawsonii. *Botanical Journal of the Linnean Society*, **124**, 345–360.

EGLINTON, G. and LOGAN, G. A. 1991. Molecular Preservation. *Philosophical Transactions of the Royal Society B: Biological Sciences*, **333**, 315–327.

FEIST, M., LIU, J. and TAFFOREAU, P. 2005. New insights into Paleozoic charophyte morphology and phylogeny. *American Journal of Botany*, **92**, 1152–1160.

FLOUDAS, D., BINDER, M., RILEY, R., BARRY, K., BLANCHETTE, R. A., HENRISSAT, B., MARTINEZ, A. T., OTILLAR, R., SPATAFORA, J. W., YADAV, J. S., AERTS, A., BENOIT, I., BOYD, A., CARLSON, A., COPELAND, A., COUTINHO, P. M., DE VRIES, R. P., FERREIRA, P., FINDLEY, K., FOSTER, B., GASKELL, J., GLOTZER, D., GORECKI, P., HEITMAN, J., HESSE, C., HORI, C., IGARASHI, K., JURGENS, J. A., KALLEN, N., KERSTEN, P., KOHLER, A., KUES, U., KUMAR, T. K. A., KUO, A., LABUTTI, K., LARRONDO, L. F., LINDQUIST, E., LING, A., LOMBARD, V., LUCAS, S., LUNDELL, T., MARTIN, R., MCLAUGHLIN, D. J., MORGENSTERN, I., MORIN, E., MURAT, C., NAGY, L. G., NOLAN, M., OHM, R. A., PATYSHAKULIYEVA, A., ROKAS, A., RUIZ-DUENAS, F. J., SABAT, G., SALAMOV, A., SAMEJIMA, M., SCHMUTZ, J., SLOT, J. C., ST. JOHN, F., STENLID, J., SUN, H., SUN, S., SYED, K., TSANG, A., WIEBENGA, A., YOUNG, D., PISABARRO, A., EASTWOOD, D. C., MARTIN, F., CULLEN, D., GRIGORIEV, I. V. and HIBBETT, D. S. 2012. The Paleozoic Origin of Enzymatic Lignin Decomposition Reconstructed from 31 Fungal Genomes. *Science*, **336**, 1715–1719.

GALVEZ, M. E., BEYSSAC, O., BENZERARA, K., MENGUY, N., BERNARD, S. and COX, S. C. 2012*a*. Micro- and nano-textural evidence of Ti(–Ca–Fe) mobility during fluid–rock interactions in carbonaceous lawsonite-bearing rocks from New Zealand. *Contributions to Mineralogy and Petrology*, **164**, 895–914.

GALVEZ, M. E., BEYSSAC, O., BENZERARA, K., BERNARD, S., MENGUY, N., COX, S. C., MARTINEZ, I., JOHNSTON, M. R. and BROWN, G. E. 2012*b*. Morphological

preservation of carbonaceous plant fossils in blueschist metamorphic rocks from New Zealand: Fossil preservation in metamorphic rocks. *Geobiology*, **10**, 118–129.

GARWOOD, R. and DUNLOP, J. 2014. The walking dead: Blender as a tool for paleontologists with a case study on extinct arachnids. *Journal of Paleontology*, **88**, 735–746.

GERRIENNE, P., GENSEL, P. G., STRULLU-DERRIEN, C., LARDEUX, H., STEEMANS, P. and PRESTIANNI, C. 2011. A Simple Type of Wood in Two Early Devonian Plants. *Science*, **333**, 837–837.

GRIMES, S. T., BROCK, F., RICKARD, D., DAVIES, K. L., EDWARDS, D., BRIGGS, D. E. G. and PARKES, R. J. 2001. Understanding fossilization: Experimental pyritization of plants. *Geology*, **29**, 123.

GUPTA, N. S. 2015. Plant Biopolymer–Geopolymer: Organic Diagenesis and Kerogen Formation. *Frontiers in Materials*, **2**.

HAUSRATH, E. M., NEAMAN, A. and BRANTLEY, S. L. 2009. Elemental release rates from dissolving basalt and granite with and without organic ligands. *American Journal of Science*, **309**, 633–660.

HUGGINS, F. E. and HUFFMAN, G. P. 2004. How do lithophile elements occur in organic association in bituminous coals? *International Journal of Coal Geology*, **58**, 193–204.

KARUNAKARAN, C., CHRISTENSEN, C. R., GAILLARD, C., LAHLALI, R., BLAIR, L. M., PERUMAL, V., MILLER, S. S. and HITCHCOCK, A. P. 2015. Introduction of Soft X-Ray Spectromicroscopy as an Advanced Technique for Plant Biopolymers Research. *PLOS ONE*, **10**, e0122959.

KAZNATCHEEV, K. V., KARUNAKARAN, C., LANKE, U. D., URQUHART, S. G., OBST, M. and HITCHCOCK, A. P. 2007. Soft X-ray spectromicroscopy beamline at the CLS: Commissioning results. *Nuclear Instruments and Methods in Physics Research Section A: Accelerators, Spectrometers, Detectors and Associated Equipment*, **582**, 96–99.

KEILUWEIT, M., NICO, P. S., KLEBER, M. and FENDORF, S. 2016. Are oxygen limitations under recognized regulators of organic carbon turnover in upland soils? *Biogeochemistry*, **127**, 157–171.

KENRICK, P. and EDWARDS, D. 1988. The anatomy of Lower Devonian Gosslingia breconensis Heard based on pyritized axes, with some comments on the permineralization process. *Botanical Journal of the Linnean Society*, **97**, 95–123.

KENRICK, P. and CRANE, P. R. 1997. The origin and early evolution of plants on land. *Nature*, **389**, 33.

KRAH, F.-S., BÄSSLER, C., HEIBL, C., SOGHIGIAN, J., SCHAEFER, H. and HIBBETT, D. S. 2018. Evolutionary dynamics of host specialization in wood-decay fungi. *BMC Evolutionary Biology*, **18**.

LE GUILLOU, C., BERNARD, S., DE LA PENA, F. and LE BRECH, Y. 2018. XANES-Based Quantification of Carbon Functional Group Concentrations. *Analytical Chemistry*, **90**, 8379–8386.

LEHMANN, J. and KLEBER, M. 2015. The contentious nature of soil organic matter. *Nature*, **528**, 60.

LEKELE BAGHEKEMA, S. G., LEPOT, K., RIBOULLEAU, A., FADEL, A., TRENTESAUX, A. and EL ALBANI, A. 2017. Nanoscale analysis of preservation of ca. 2.1 Ga old Francevillian microfossils, Gabon. *Precambrian Research*, **301**, 1–18.

LEPOT, K., BENZERARA, K., BROWN, G. E. and PHILIPPOT, P. 2008. Microbially influenced formation of 2,724-million-year-old stromatolites. *Nature Geoscience*, **1**, 118–121.

LI, J., BENZERARA, K., BERNARD, S. and BEYSSAC, O. 2013. The link between biomineralization and fossilization of bacteria: Insights from field and experimental studies. *Chemical Geology*, **359**, 49–69.

LI, J., BERNARD, S., BENZERARA, K., BEYSSAC, O., ALLARD, T., COSMIDIS, J. and MOUSSOU, J. 2014. Impact of biomineralization on the preservation of microorganisms during fossilization: An experimental perspective. *Earth and Planetary Science Letters*, **400**, 113–122.

LIMAYE, A. 2012. Drishti: a volume exploration and presentation tool. Proc. SPIE 8506 Developments in X-Ray Tomography VIII; 85060X. doi: 10.1117/12.935640.

NELSEN, M.P., DIMICHELE, W.A., PETERS, S.E. and BOYCE, C.K. 2016. Delayed fungal evolution did not cause the Paleozoic peak in coal production. Proceedings *s of the National Academy of Sciences* USA **113**, 2442–2447.

MA, J., ZHANG, K., HUANG, M., HECTOR, S. B., LIU, B., TONG, C., LIU, Q., ZENG, J., GAO, Y., XU, T., LIU, Y., LIU, X. and ZHU, Y. 2016. Involvement of Fenton chemistry in rice straw degradation by the lignocellulolytic bacterium Pantoea ananatis Sd-1. *Biotechnology for Biofuels*, **9**.

MCNAMARA, M. E., BRIGGS, D. E. G., ORR, P. J., FIELD, D. J. and WANG, Z. 2013*a*. Experimental maturation of feathers: implications for reconstructions of fossil feather colour. *Biology Letters*, **9**, 20130184–20130184.

MCNAMARA, M. E., BRIGGS, D. E. G., ORR, P. J., GUPTA, N. S., LOCATELLI, E. R., QIU, L., YANG, H., WANG, Z., NOH, H. and CAO, H. 2013*b*. The fossil record of insect color illuminated by maturation experiments. *Geology*, **41**, 487–490.

MIOT, J., BERNARD, S., BOURREAU, M., GUYOT, F. and KISH, A. 2017. Experimental maturation of Archaea encrusted by Fe-phosphates. *Scientific Reports*, **7**.

PE-PIPER, G., KARIM, A. and PIPER, D. J. W. 2011. Authigenesis of Titania Minerals and the Mobility of Ti: New Evidence From Pro-Deltaic Sandstones, Cretaceous Scotian Basin, Canada. *Journal of Sedimentary Research*, **81**, 762–773.

RAMAKRISHNA, R. S., PAUL, A. A. and FONSEKA, J. P. R. 1989. Uptake of titanium and iron by Ipomoea biloba from titaniferrous sands. *Environmental and Experimental Botany*, **29**, 293–300.

RUMBLE, D., DUKE, E. F. and HOERING, T. L. 1986. Hydrothermal graphite in New Hampshire: Evidence of carbon mobility during regional metamorphism. *Geology*, **14**, 452.

SCHIFFBAUER, J. D. and XIAO, S. 2009. Novel application of focused ion beam electron microscopy (FIB-EM) in preparation and analysis of microfossil ultrastructures: A new view of complexity in early Eukaryotic organisms. *PALAIOS*, **24**, 616–626.

SCHIFFBAUER, J. D., WALLACE, A. F., HUNTER, J. L., KOWALEWSKI, M., BODNAR, R. J. and XIAO, S. 2012. Thermally-induced structural and chemical alteration of organic-walled microfossils: an experimental approach to understanding fossil preservation in metasediments: Experimental thermal alteration of microfossils. *Geobiology*, **10**, 402–423.

SCHIFFBAUER, J. D., XIAO, S., CAI, Y., WALLACE, A. F., HUA, H., HUNTER, J., XU, H., PENG, Y. and KAUFMAN, A. J. 2014. A unifying model for Neoproterozoic–Palaeozoic exceptional fossil preservation through pyritization and carbonaceous compression. *Nature Communications*, **5**.

SCHMIDT, M. W. I., TORN, M. S., ABIVEN, S., DITTMAR, T., GUGGENBERGER, G., JANSSENS, I. A., KLEBER, M., KÖGEL-KNABNER, I., LEHMANN, J., MANNING, D. A. C., NANNIPIERI, P., RASSE, D. P., WEINER, S. and TRUMBORE, S. E. 2011. Persistence of soil organic matter as an ecosystem property. *Nature*, **478**, 49–56.

STEEMANS, P., LEPOT, K., MARSHALL, C. P., LE HÉRISSÉ, A. and JAVAUX, E. J. 2010. FTIR characterisation of the chemical composition of Silurian miospores (cryptospores and trilete spores) from Gotland, Sweden. *Review of Palaeobotany and Palynology*, **162**, 577–590.

STRULLU-DERRIEN, C. 2010. *Recherches sur la colonisation du milieu terrestre par les plantes au cours du Dévonien inférieur et sur les interactions plantes/microorganismes durant les périodes Dévonien-Carbonifère*. PhD Thesis. University of Angers.

STRULLU-DERRIEN, C., KENRICK, P., BADEL, E., COCHARD, H. and TAFFOREAU, P. 2013. An overview of the hydraulic systems in early land plants. *IAWA Journal*, **34**, 333–351.

STRULLU-DERRIEN, C., KENRICK, P., TAFFOREAU, P., COCHARD, H., BONNEMAIN, J.-L., LE HÉRISSÉ, A., LARDEUX, H. and BADEL, E. 2014. The earliest wood and its hydraulic properties documented in *c* . 407-million-year-old fossils using synchrotron microtomography: Hydraulic Properties of Earliest Wood. *Botanical Journal of the Linnean Society*, **175**, 423–437.

STRULLU-DERRIEN, C., DUCASSOU, C., BALLÈVRE, M., DABARD, M.-P., GERRIENNE, P., LARDEUX, H., LE HÉRISSÉ, A., ROBIN, C., STEEMANS, P. and STRULLU, D.-G. 2010. The early land plants from the Armorican Massif: sedimentological and palynological considerations on age and environment. *Geological Magazine*, **147**, 830–843.

SWARAJ, S., BELKHOU, R., STANESCU, S., RIOULT, M., BESSON, A. and HITCHCOCK, A. P. 2017. Performance of the HERMES beamline at the carbon K-edge. *Journal of Physics: Conference Series*, **849**, 012046.

TEGELAAR, E. ., DE LEEUW, J. ., DERENNE, S. and LARGEAU, C. 1989. A reappraisal of kerogen formation. *Geochimica et Cosmochimica Acta*, **53**, 3103–3106.

VAN BERGEN, P. F., COLLINSON, M. E., BRIGGS, D. E. G., DE LEEUW, J. W., SCOTT, A. C., EVERSHED, R. P. and FINCH, P. 1995. Resistant biomacromolecules in the fossil record [1]. *Acta Botanica Neerlandica*, **44**, 319–342.

VINOGRADOFF, V., BERNARD, S., LE GUILLOU, C. and REMUSAT, L. 2018. Evolution of interstellar organic compounds under asteroidal hydrothermal conditions. *Icarus*, **305**, 358–370.

WACEY, D., SAUNDERS, M. and KONG, C. 2018. Remarkably preserved tephra from the 3430 Ma Strelley Pool Formation, Western Australia: Implications for the interpretation of Precambrian microfossils. *Earth and Planetary Science Letters*, **487**, 33–43.

WANG, J., MORIN, C., LI, L., HITCHCOCK, A. P., SCHOLL, A. and DORAN, A. 2009. Radiation damage in soft X-ray microscopy. *Journal of Electron Spectroscopy and Related Phenomena*, **170**, 25–36.

WILHELM, R. C., SINGH, R., ELTIS, L. D. and MOHN, W. W. 2018. Bacterial contributions to delignification and lignocellulose degradation in forest soils with metagenomic and quantitative stable isotope probing. *The ISME Journal*.

WIRTH, R. 2009. Focused Ion Beam (FIB) combined with SEM and TEM: Advanced analytical tools for studies of chemical composition, microstructure and crystal structure in geomaterials on a nanometre scale. *Chemical Geology*, **261**, 217–229.

EXPLANATIONS OF FIGURES

FIG. 1. Geological and mineralogical context. **a.** Picture of a specimen of *A. chateaupannense* preserved in 2D as carbonaceous thin films. **b.** SEM image of a transverse section of an axis of a specimen of *A. chateaupannense* preserved in 3D showing the radially aligned tracheids. **c.** Lithostratigraphic column of the Chateaupanne unit (after Strullu-Derrien et al., 2010, 2014). **d.** Location of the plant-rich level containing the specimens investigated (after Strullu-Derrien et al., 2010, 2014). Scale bar is 4 km.

FIG. 2. Composition of the mineral matrix. **a.** STEM image in HAADF mode (z-contrast) showing the heterogeneous nature of the mineral matrix. **b.** STEM image of another area of the mineral matrix and corresponding EDXS maps showing the spatial distribution of silicon, aluminium, iron, potassium, phosphorus and titanium. **c.** EDX spectra of Ti-oxides, Fe-silicates, K-silicates, Al-(Ce-)phosphates and Si-minerals (quartz). Scale bars are 1 µm (a,b).

FIG. 3. Microstructure of the specimens preserved in 3D. **a.** Part of a reconstructed 3D bloc of *A. chateaupannense* preserved in 3D. **b.** Organic structure of the P-type tracheid cells. **c.** Detail of b. **d.** Area showing the scalariform bordered pits of the tracheids. **e.** Detail of d. **f.** Area showing the perforate sheet of secondary wall material overlying the pit apertures. **g.** Detail of f. **h-i.** Inside views of a tracheid. Scale bars: a–d = 100 µm, e–g = 50 µm, h,i= 25 µm.

FIG. 4. Geochemical nature of the investigated specimens. **a.** C-XANES spectra of the organic carbon of a specimen preserved in 3D (red) and of a specimen preserved in 2D (blue). C-XANES spectra of pyrobitumen (Bernard and Horsfield 2014) and lignin (Bernard *et al.* 2010) are shown for comparison. **f.** High resolution STEM image of the organic carbon (dark) of a specimen preserved in 3D showing the automorphic nature of the Ti-minerals (bright). **b.** STEM image of

the organic carbon of a specimen preserved in 3D. Organic carbon appears dark while automorphic Ti-nanominerals appear bright. **c.** STEM image of the organic carbon of a specimen preserved in 2D. Organic carbon appears dark while Ti-, Fe- and Ca-nanominerals appear bright. **d.** EDXS compositional map of the area located by a red square in c, showing the spatial distribution of organic carbon (carbon appears in black), oxyhydroxide minerals (iron appears in red), calcite minerals (calcium appears in green) and Ti-nanominerals (titanium appears in blue). **e.** STEM image of the organic carbon of a specimen preserved in 3D. Organic carbon appears dark while Ti-nanominerals appear bright. **f.** EDX spectra of the organic compounds (similar for the specimens preserved in 2D and in 3D), Ti-nanominerals (similar for the specimens preserved in 2D and in 3D), Ca-nanominerals (only observed in the specimens preserved in 2D) and Fe-nanominerals (only observed in the specimens preserved in 2D). Scale bars are 200 nm (b) and 500 nm (c,d,e).

SUPPLEMENTARY MATERIAL

MOVIE S1: 3D view of a tracheid.

DATA ARCHIVING STATEMENT

Data for this study are available in the Zenodo repository: http://dx.doi.org/10.5281/zenodo.1290504

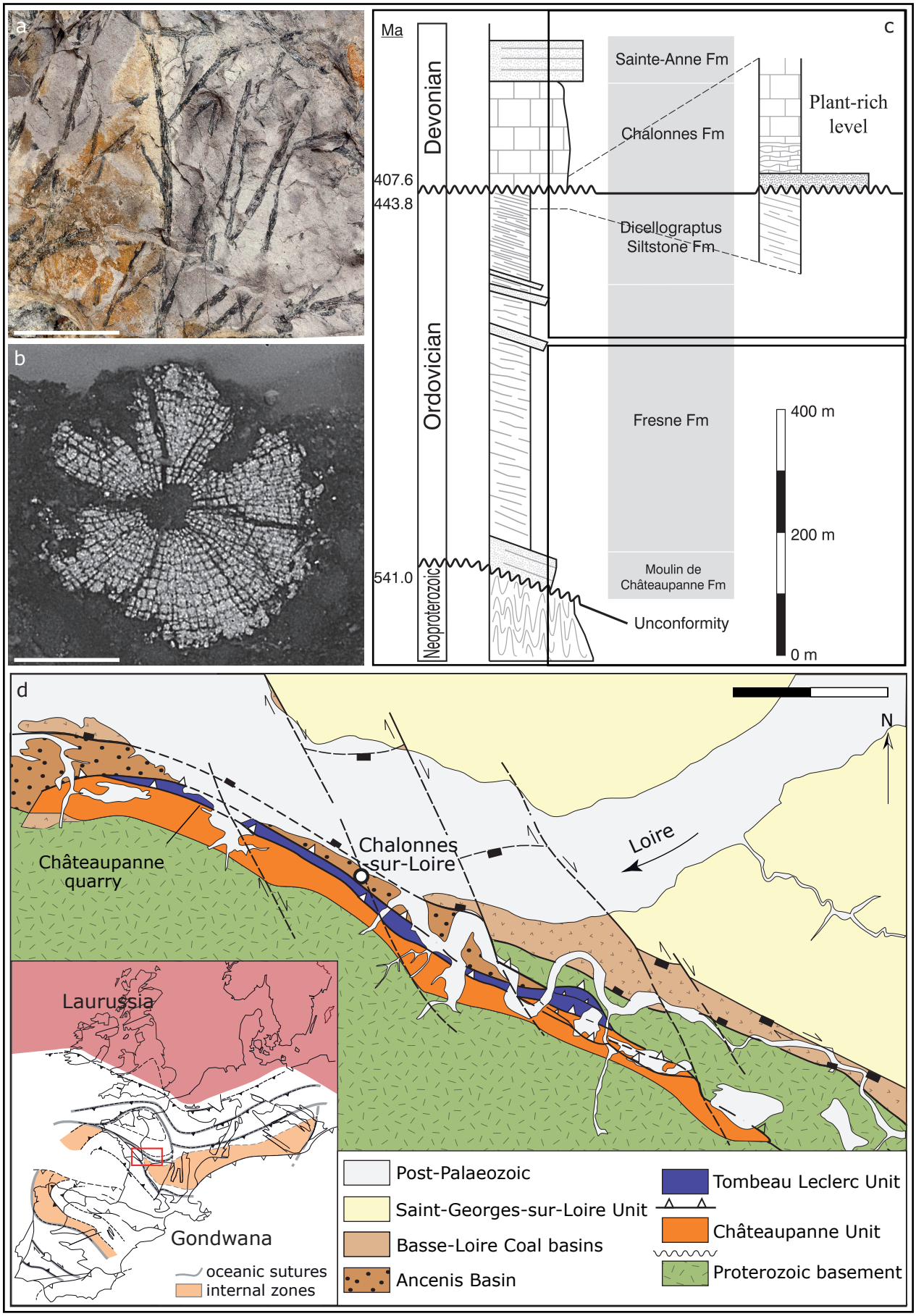
a
b
c
Ma
Devonian
Ordovician
Neoproterozoic
407.6
443.8
541.0
Sainte-Anne Fm
Chalonnes Fm
Dicellograptus Siltstone Fm
Fresne Fm
Moulin de Châteaupanne Fm
Unconformity
Plant-rich level
400 m
200 m
0 m
d
N
Loire
Chalonnes-sur-Loire
Châteaupanne quarry
Laurussia
Gondwana
oceanic sutures
internal zones
Post-Palaeozoic
Saint-Georges-sur-Loire Unit
Basse-Loire Coal basins
Ancenis Basin
Tombeau Leclerc Unit
Châteaupanne Unit
Proterozoic basement

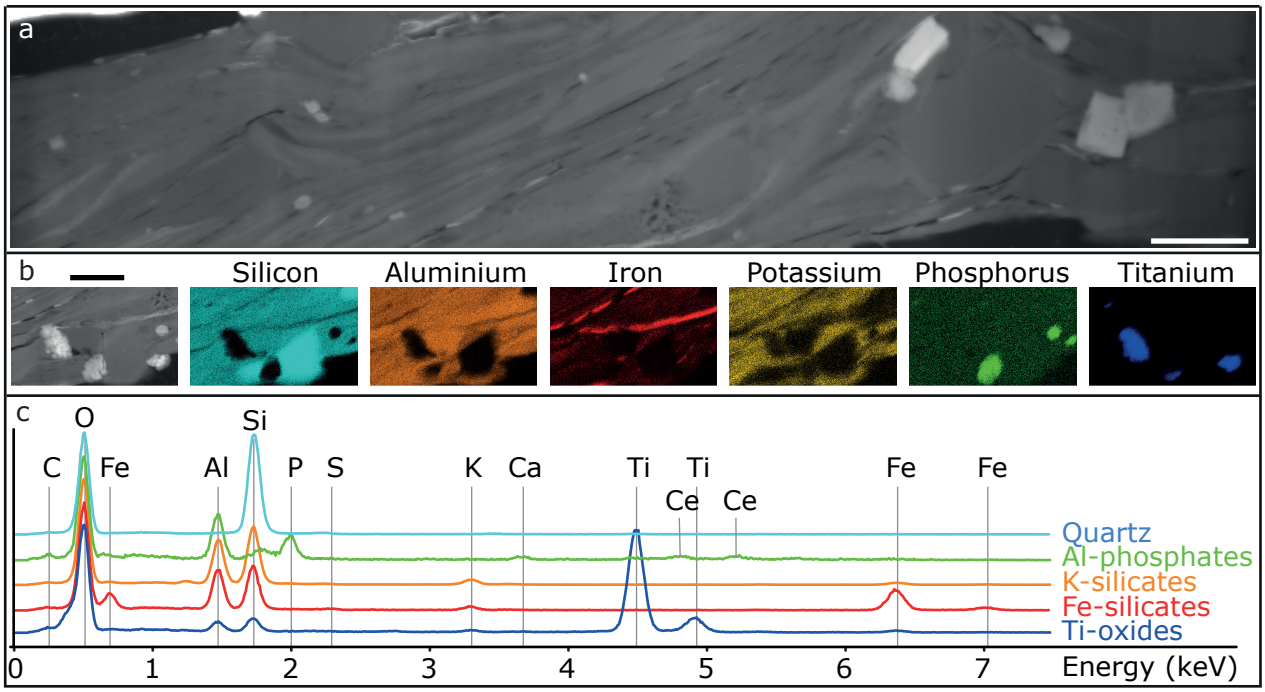
a
b
Silicon
Aluminium
Iron
Potassium
Phosphorus
Titanium
c
O
Si
C
Fe
Al
P
S
K
Ca
Ti
Ti
Ce
Ce
Fe
Fe
Quartz
Al-phosphates
K-silicates
Fe-silicates
Ti-oxides
0
1
2
3
4
5
6
7
Energy (keV)

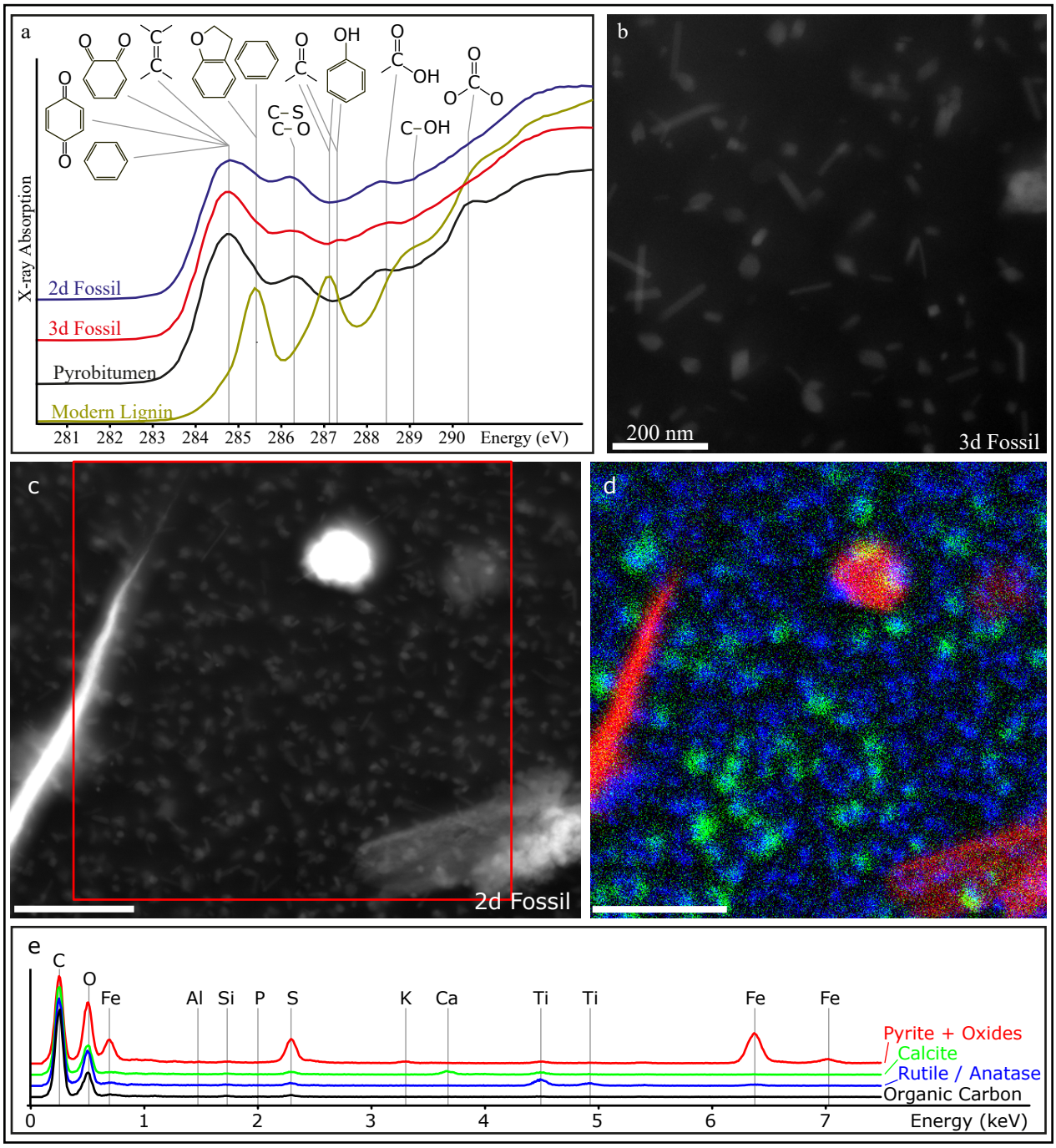
a
C–S
C–O
C–OH
X-ray Absorption
2d Fossil
3d Fossil
Pyrobitumen
Modern Lignin
281 282 283 284 285 286 287 288 289 290 Energy (eV)
b
200 nm
3d Fossil
c
2d Fossil
d
e
C
O
Fe
Al Si P S
K Ca
Ti Ti
Fe Fe
Pyrite + Oxides
Calcite
Rutile / Anatase
Organic Carbon
0 1 2 3 4 5 6 7 Energy (keV)